The Accuracy of RTK enabled Mobile Phones in RTK denied Areas

Christoph Strecha[1], Martin Rehak[1], Davide Cucci [1]

[1] Pix4D SA. Route de Renens 24 1008 Prilly, Switzerland (christoph.strecha@pix4d.com, martin.rehak@pix4d.com, davide.cucci@pix4d.com)

Keywords: iPhone LiDAR, RTK, GNSS, Surveying.

Abstract

Surveyors often encounter challenges when tasked with measuring points in regions where buildings disrupt satellite visibility. The precise surveying of points in these areas typically relies on employing total stations. This method effectively extends high precision from unaffected zones (where satellite visibility is assured) to those areas where disruption occurs due to buildings. Total stations achieve this by executing distance and angle measurements from a reference point coordinate to the location where satellite visibility is compromised. The process is notably time-consuming, thereby incurring significant costs. Moreover, the intricate nature of this surveying process necessitates specialized skills and expertise, contributing further to the overall expense. In this study, we investigate an approach based on RTK (Real-Time Kinematic) enabled mobile phones and photogrammetry to achieve the same. In principle, this approach has a similar philosophy. However, instead of working with a few points with good satellite visibility that are obtained by a GNSS (Global Navigation Satellite System) rover, the procedure works with hundreds of observations with varying accuracy. Those accuracies depend on the satellite visibility. Each observation captures an image from the mobile phone together with the GNSS signal and its accuracy. Angle and distance measurements that traditionally are observed by a total station are retrieved by photogrammetry on the total image collection.

1. Introduction

Mobile phones are becoming an important tool for geoscience. Several studies on this topic evaluate the accuracy and applicability of widespread mobile phones for dedicated industries and applications. Prior research focuses on 1) photogrammetry techniques using mobile phone imagery (Dzelzkaleja et al., 2021, Bessin et al., 2023), 2) the use of the LiDAR sensor available in modern Apple phones (Pluta and Siemek, 2024, Guenther et al., 2024, Kottner et al., 2023, Rutkowski and Lipecki, 2023, Hakim et al., 2023), and 3) the combination of both LiDAR and photogrammetry from these mobile phones (Barrile et al., 2022, Błaszczak-Bak et al., 2023), as well as overview research (Corradetti et al., 2022).

Interesting research is also available in the study combining well-known UAV imagery with ground-based photogrammetry from mobile phones (Kovanič et al., 2023). Recently, several new GNSS RTK rovers have become available (Emlid, 2024, Trimble, 2022, vigram, 2024). These devices can seamlessly connect to a mobile device and enable accurate geotagging of images, bringing the professional usage of mobile phones to another level. 3D models from mobile phones are not only visually appealing digital twins but can also be geo-referenced with survey-grade absolute accuracy. This also makes it possible to easily combine mobile phone data with drone data captured with RTK/PPK technology.

In many urban scenarios, surveyors face difficulty measuring points in areas where satellite visibility is obstructed by buildings. In this study, we evaluate RTK-enabled mobile phones and photogrammetry, which claim to achieve cm-level mapping accuracy in these areas (Pix4D, 2021). The approach is conceptually similar to the traditional method using a total station. However, instead of relying on a few points with good satellite visibility obtained by a GNSS rover, this procedure works with hundreds of observations of varying accuracy. These accuracies depend on the satellite visibility at each particular location. Each observation captures an image from the mobile phone along with the GNSS signal and its accuracy. Angle and distance measurements traditionally obtained by a total station are retrieved by photogrammetry from the total image collection.

Figure 1 shows the situation in a real example. One can see the image positions as red ellipsoids, with the size of the ellipsoid representing the accuracy of the GNSS signal for each image. A surveying point (pink cone) is observed by many images. The image observations are shown on the right, and the connections from the survey point to the images where that point is seen are visualized on the left by yellow lines. Direct measurements of distances and angles are replaced by photogrammetric triangulation as visualized in Figure 1. Instead of surveying single points, this approach builds a photogrammetric network of hundreds of images tied to the GNSS measurements of each image. In areas with good GNSS accuracy, images are more strongly tied to the GNSS positions, while in areas with weak (or missing) GNSS signals, the images are more closely tied to their neighboring images in the photogrammetric network.

In this study, we evaluate a new algorithm that fuses GNSS information with sensors measuring the relative movement of the mobile phone. This algorithm runs inside a mobile phone app that automatically captures images and collects GNSS signals with the RTK phone add-on seen in Figure 2. We use the Emlid RX (Emlid, 2024) for all our experiments.

Consumer devices used in workflows for professionals are very interesting because of their ease of use and price. Drones, initially designed for consumer applications, are today part of the surveyor’s toolbox. They do not replace traditional surveying equipment completely, but more and more professional tasks are performed with these devices. It is therefore not surprising that previous work has studied the performance of the LiDAR sensor present in the newer versions of the iPhone, e.g. ,(Luetzenburg et al., 2021, Hakim

This contribution has been peer-reviewed. The double-blind peer-review was conducted on the basis of the full paper.
https://doi.org/10.5194/isprs-annals-X-4-2024-327-2024

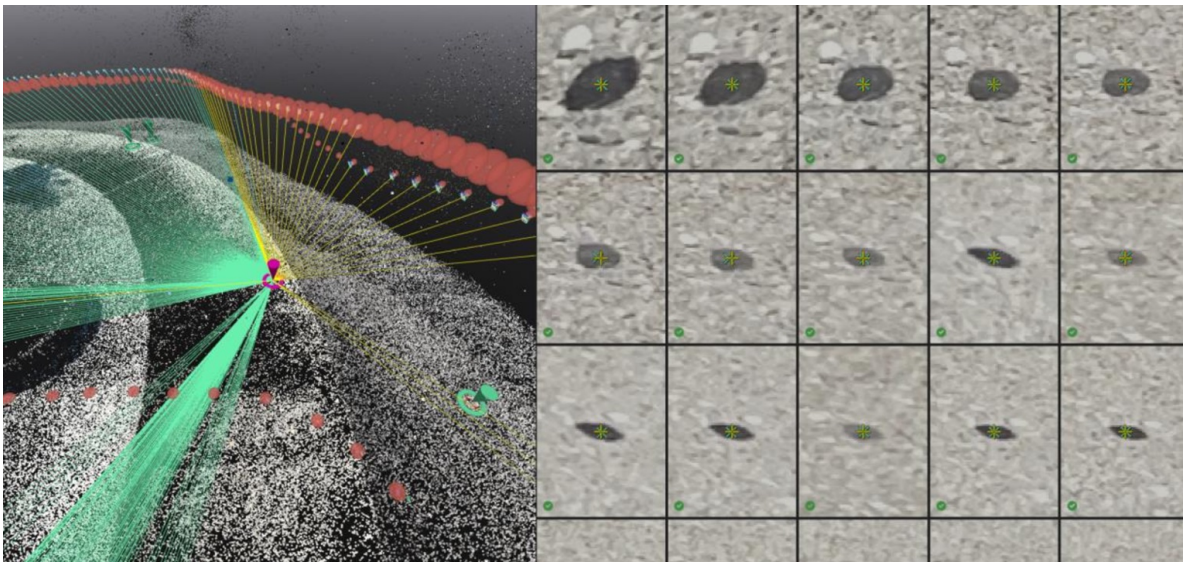

Figure 1. Screenshot of PIX4Dmatic showing image positions and their accuracies represented by red ellipsoids, together with a triangulated survey point (pink cone) obtained from image observations (shown right) by triangulation. All image observations and the survey points are connected by yellow lines.

Figure 2. iPhone with PIX4Dcatch connected to the RTK device: Emlid RX (left). Covering the antenna (right) simulates the loss of RTK fix in the same scene with measured check points.

et al., 2023) and (Teppati Losè et al., 2022). In the work here, we focus additionally on the global accuracy that can be obtained by adding an external RTK device to the iPhone.

2. Surveying with Mobile Phones and RTK add-on

For our survey, we use the Apple iPhone 14 Pro, on which the free application PIX4Dcatch (Pix4D, 2021) is installed. After registering with Pix4D, we could in principle start data collection. However, this will only use the internal GNSS sensor with an approximate accuracy of 2-5m. To achieve survey-grade accuracy, we added an RTK device to the phone via the widely used SPC+ connector (SP-Connect, 2024). This whole setup is shown in Figure 2 (left). The mobile phone app PIX4Dcatch connects via Bluetooth to the Emlid RX. The NTRIP (Networked Transport of RTCM via Internet Protocol) service can be connected, and the system is ready to be used. When starting acquisition inside PIX4Dcatch, images (and in the case of the iPhone, also LiDAR data) are automatically captured while moving through the survey area. The images and LiDAR are triggered based on distance (e.g., every 20cm) or based on overlap of the images. Images and RTK information from the Emlid RX are synchronized, and when the acquisition is finished, all data is optimized by the GeoFusion algorithm running inside PIX4Dcatch, which puts the computed positions, accuracies, and orientations into the EXIF of the images. GeoFusion uses the available information about position and orientation coming from the phone as well as the information from the Emlid RX GNSS receiver. The optimization also uses the information about the accuracy of all data. It is capable of mitigating temporal GNSS outages or losses of RTK FIX solutions in order to maintain cm-level accuracy throughout the entire project.

Figure 3. Open test fields with 7 check points (green) and the mobile phone path (blue).

It is important to notice, and this is the main advantage of the system for surveying points in regions with poor GNSS signal quality, that the mobile phone is equipped with relatively good

This contribution has been peer-reviewed. The double-blind peer-review was conducted on the basis of the full paper.
https://doi.org/10.5194/isprs-annals-X-4-2024-327-2024 | © Author(s) 2024. CC BY 4.0 License.

sensors and algorithms to track its orientation and position while moving. Over longer distances, this tracking system does suffer from drifting. However, the drift is compensated by the RTK positions from the Emlid RX. The main question here is whether the tracking of the phone in the short range can compensate for potential inaccuracies due to RTK outages. If this is possible, we are equipped with an easy-to-use solution for surveying points in urban canyon scenarios.

3. Experimental Setup

We use for the experiments an urban test field where satellite visibility is not heavily disturbed by large buildings and an area close to buildings. Check points of known location have been set up and measured with a professional survey-grade GNSS rover. The accuracy of these points is 1.5 cm horizontally and 2 cm vertically, respectively. For the first test field, one can see the satellite image of the area, and those 7 check points are shown in Figure 3. The second test field is shown in Figure 5 and is equipped with 8 check points. In order to assess the accuracy in RTK denied areas, we simulate the loss of RTK fix of our device by blocking the antenna during the data acquisition in the first test area. This results in a temporary loss of RTK fix and a loss of accuracy of the GNSS readings. However, Pix4D’s approach to solving these problems is their GeoFusion algorithm. In Section 4, we evaluate the accuracy of GeoFusion itself, and in Section 4, how the accuracy behaved when running a full photogrammetric block adjustment with images and LiDAR in addition to the GeoFusion output.

For these experiments, we collected two datasets: one in which the antenna was not covered and thus had RTK fix for all images, and one in which the antenna was covered. You can see the XY and Z accuracy for these two acquisitions in Figure 4. The accuracies are reported by the RTK device, which in this case was the Emlid RX (PIX4Dmatic reports these accuracies as error ellipsoids in red, see Figure 10). The second test area depicted in Figure 5 suffers from poor satellite visibility, as seen in the accuracy output in Figure 6. Notice the asymmetric shape of the peaks. When uncovering the antenna, position accuracy increases rapidly, but it takes some time before the RTK is fixed.

4. Experiments

The data acquisition was carried out with an iPhone running the mobile app PIX4Dcatch, which handles the connection to the RTK add-on, resulting in a set of images, LiDAR, and LiDAR confidence maps. The images are geotagged with the position and orientation obtained from GeoFusion. Since the camera internals are also known approximately, one can import the check points into PIX4Dmatic and mark them in the images before any photogrammetric processing is performed. Figures 7 and 8 show screenshots of both datasets after marking the check points inside the images. The table below shows the XYZ error on the measured check points and the points obtained from triangulating the image marks. Note that for the triangulation, PIX4Dmatic uses the camera internals, as well as the positions and orientations obtained from the EXIF (Exchangeable Image File format) data written by PIX4Dcatch after running the GeoFusion on the mobile phone. This process does not require any photogrammetric processing. PIX4Dmatic is only used to manage the check points,

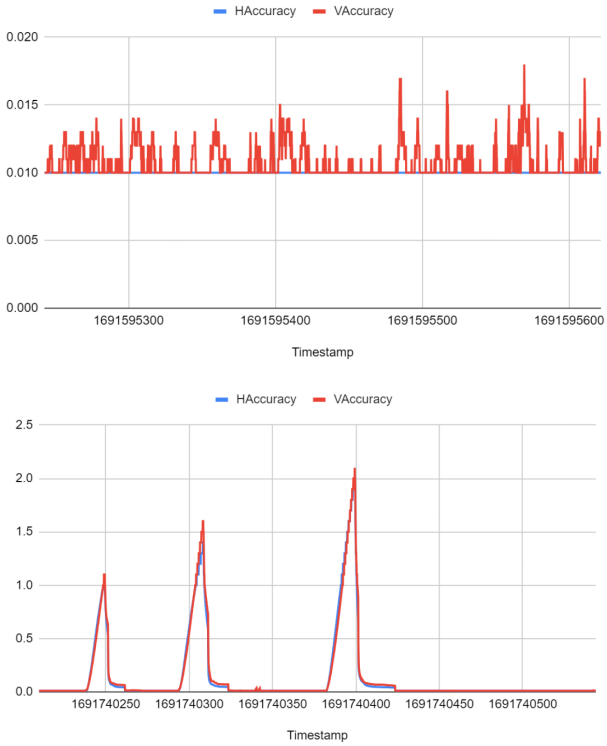

Figure 4. XY and Z accuracies of the two datasets. Top: RTK fix throughout the whole acquisition. Bottom: during the acquisition, the antenna was covered three times, clearly visible as spikes.

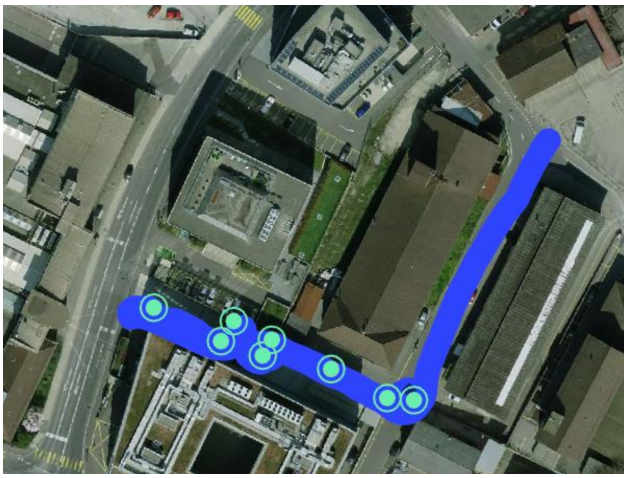

Figure 5. Test field close to buildings with check points (green) and the camera path (blue).

coordinate system, and triangulation of image marks. The RMS error for the three datasets can be found in Table 1.

Without photogrammetric processing, the RMS error for the RTK fix dataset is about 5 cm on those 7 check points. If the antenna is covered and the RTK fix is lost, the RMS error is 15 cm. We report these results here to understand the performance of the GeoFusion algorithm. This is particularly interesting given that this algorithm runs in near real-time on a mobile phone. Accuracy of this level opens new possibilities for using

This contribution has been peer-reviewed. The double-blind peer-review was conducted on the basis of the full paper.
https://doi.org/10.5194/isprs-annals-X-4-2024-327-2024 | © Author(s) 2024. CC BY 4.0 License.

	RMS X [m]	RMS Y [m]	RMS Z [m]	Average [m]
Dataset 1 (good visibility)	0.046	0.047	0.046	0.046
Dataset 2 (covered antenna)	0.190	0.081	0.161	0.144
Dataset 3 (close to buildings)	0.052	0.055	0.047	0.052

Table 1. RMS error for the three datasets without photogrammetric processing.

	RMS X [m]	RMS Y [m]	RMS Z [m]	Average [m]
Dataset 1 (good visibility)	0.038	0.011	0.031	0.027
Dataset 2 (covered antenna)	0.027	0.020	0.061	0.036
Dataset 3 (close to buildings)	0.033	0.027	0.014	0.024

Table 2. RMS error for the three datasets after photogrammetric processing in X, Y and Z.

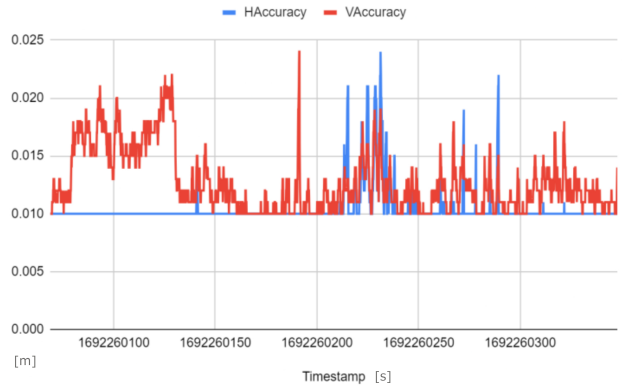

Figure 6. XY and Z accuracies for the second test field dataset. Note that since the data is collected close to a high building, we can see variations in the accuracy depending on the visibility of the satellites.

consumer-grade mobile devices in real-time applications, such as augmented reality in domains like construction site monitoring or inspections.

5. Accuracy of the Photogrammetric Block Adjustment

In this section, we present the results from photogrammetric processing. Once the PIX4Dcatch projects are imported into PIX4Dmatic, the photogrammetric processing can be launched. First, image features are matched between image pairs, and a complete bundle block adjustment is performed. This adjustment takes the RTK positions from GeoFusion, as well as their accuracies, and adjusts this information with the image-based correspondences that are automatically established. PIX4Dmatic further allows the introduction of manual tie points (MTP) and can use them in the block adjustment. After this process, we obtain refined positions, orientations, and internal parameters of the images. The accuracies of the RTK positions tie the images closer to the RTK positions with high accuracy, whereas in areas with lower accuracy, the image-based correspondences will automatically be trusted more. By this, given that we have established many image correspondences, areas with low RTK accuracy are influenced by the high-accuracy positions in other areas.

Table 2 shows the RMS errors after photogrammetric block adjustment. The RMS error of the 7 check points decreases with the additional information from the image correspondences. One can see that the improvement is relatively stronger for the second dataset when comparing Table 1 and Table 2. In dataset 1, we already have relatively good accuracy since the GeoFusion algorithm run with very precise RTK positioning. The improvement of a photogrammetric bundle adjustment is substantial but less pronounced when compared to dataset 2. Here, inaccurate RTK positions have a larger influence, and photogrammetric image correspondences add relatively more value to the overall accuracy.

6. Conclusions

The method described in this paper can be used in scenarios where part of the scene is hidden from GNSS satellites, such as in tunnels. RTK accuracy can be obtained outside the tunnel area and propagated using the iPhone’s relative position and orientation sensors, as well as photogrammetry techniques. It was demonstrated that centimeter-level accuracy is achievable without ground control points even if the RTK fix is temporarily lost. This situation can occur in urban canyons or areas with poor GSM network coverage, resulting in outages of the RTK corrections.

Mapping with a mobile phone presents a new method for acquiring accurate geospatial data. Similar to the rise of drones used for surveying, mobile phones with RTK adapters will also become part of a surveyor’s toolbox due to their affordability, ease of use, and the accurate mapping outputs they generate when paired with the right software tools.

References

Barrile, V., Bernardo, E., Fotia, A., Bilotta, G., 2022. Integration of Laser Scanner, Ground-Penetrating Radar, 3D Models and Mixed Reality for Artistic, Archaeological and Cultural Heritage Dissemination. *Heritage*, 5, 1529-1550.

Bessin, Z., Jaud, M., Letortu, P., Vassilakis, E., Evelpidou, N., Costa, S., Delacourt, C., 2023. Smartphone Structure-from-Motion Photogrammetry from a Boat for Coastal Cliff Face Monitoring Compared with Pléiades Tri-Stereoscopic Imagery and Unmanned Aerial System Imagery. *Remote Sensing*, 15, 3824.

Błaszczak-Bak, W., Suchocki, C., Kozakiewicz, T., Janicka, J., 2023. Measurement methodology for surface defects inventory of building wall using smartphone with light detection and ranging sensor. *Measurement*, 219, 113286.

Corradetti, A., Seers, T., Mercuri, M., Calligaris, C., Busetti, A., Zini, L., 2022. Benchmarking Different SfM-MVS Photogrammetric and iOS LiDAR Acquisition Methods for the Digital Preservation of a Short-Lived Excavation: A Case Study

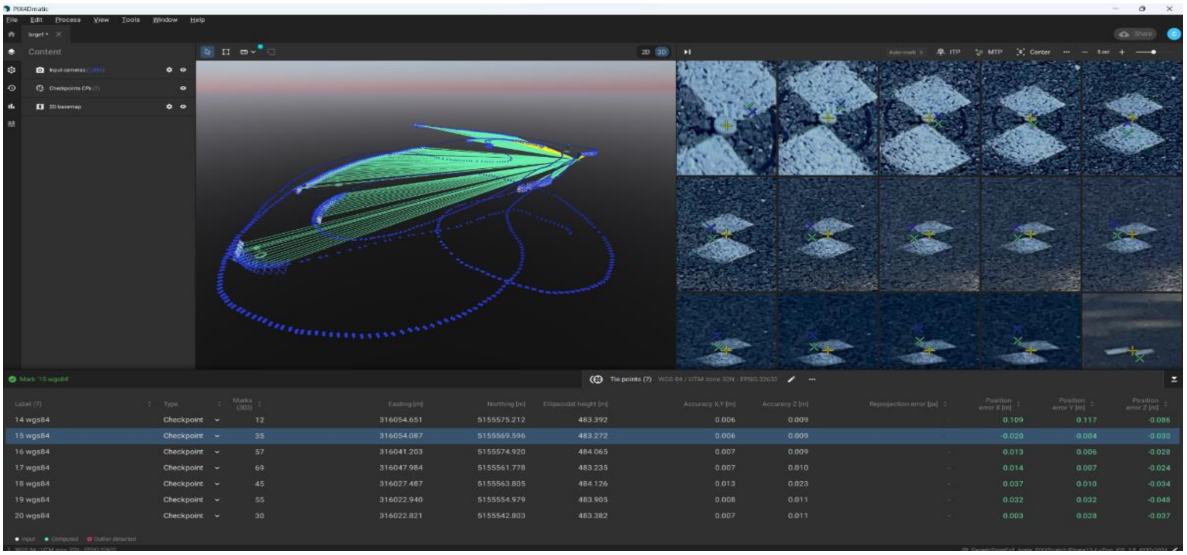

Figure 7. Marking Checkpoints inside PIX4Dmatic. Dataset 1 with complete RTK fix.

Figure 8. Importing and marking Checkpoints inside PIX4Dmatic. Dataset 2 with partial coverage of the antenna and higher uncertainty of the image positions (visible here as red ellipsoids).

from an Area of Sinkhole Related Subsidence. *Remote Sensing*, 14, 5187.

Dzelzkaleja, L., Knēts, J., Rozenovskis, N., Sīlītis, A., 2021. *Mobile Apps for 3D Face Scanning*. 34–50.

Emlid, 2024. https://emlid.com/reachrx/.

Guenther, M., Heenkenda, M., Morris, D., Leblon, B., 2024. Tree Diameter at Breast Height (DBH) Estimation Using an iPad Pro LiDAR Scanner: A Case Study in Boreal Forests, Ontario, Canada. *Forests*, 15, 214.

Hakim, N. A., Razali, R., Mohd Said, Abdul Rahim, M., 2023. Apple LiDAR Sensor for 3D Surveying: Tests and Results in the Cultural Heritage Domain. *International Journal of Geoinformatics*, 19, 79.

Kottner, S., Thali, M., Gascho, D., 2023. Using the iPhone’s LiDAR technology to capture 3D forensic data at crime and crash scenes. *Forensic Imaging*, 32, 200535.

Kovanič, , Štroner, M., Blistan, P., Urban, R., Boczek, R., 2023. Combined ground-based and UAS SfM-MVS approach for determination of geometric parameters of the large-scale industrial facility – Case study. *Measurement*, 216, 112994.

Luetzenburg, G., Kroon, A., Bjørk, A., 2021. Evaluation of the Apple iPhone 12 Pro LiDAR for an Application in Geosciences. *Scientific Reports*, 11.

Pix4D, 2021. https://www.pix4d.com/product/pix4dcatch/.

Pluta, P., Siemek, D., 2024. Possibilities and limitations of using iPhone 13 Pro with built-in LiDAR sensor in cave

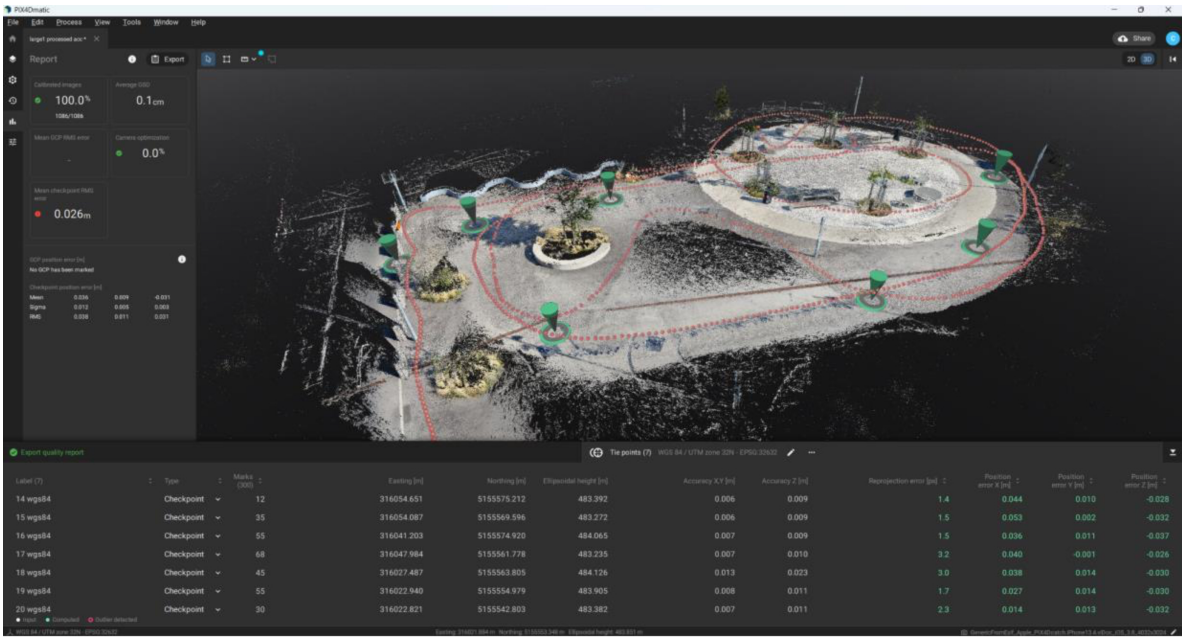

Figure 9. Dataset 2 after photogrammetric bundle adjustment. We see the dense point cloud from photogrammetry together with the colored LiDAR point cloud from the iPhone. In red are the image error ellipsoids and the check points in green.

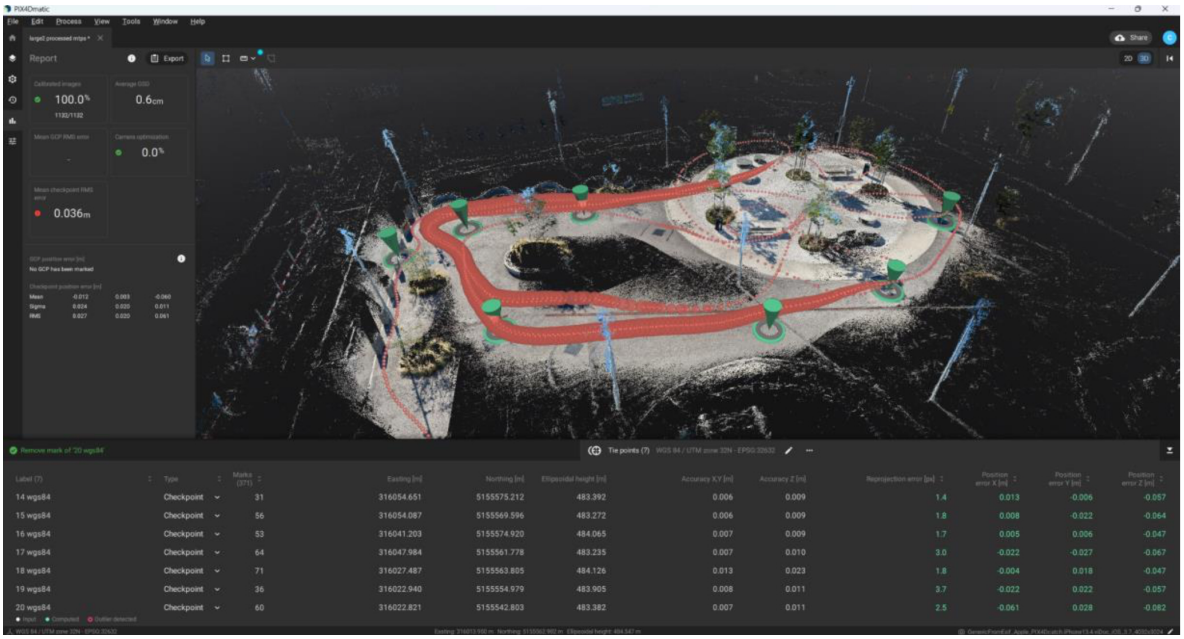

Figure 10. Dataset 2 after photogrammetric bundle adjustment. We see the dense point cloud from photogrammetry together with the colored LiDAR point cloud from the iPhone. In red are the image error ellipsoids and the check points in green. Please note the times without RTK fix (see Figure 6) in red.

research -on the example of paleoflow analysis in Mylna Cave (Western Tatra Mts, Poland). *Landform Analysis*, 42, 51-62.

Rutkowski, W., Lipecki, T., 2023. Use of the iPhone 13 Pro LiDAR Scanner for Inspection and Measurement in the Mineshaft Sinking Process. *Remote Sensing*, 15, 5089.

SP-Connect, 2024. https://sp-connect.com.

Teppati Losè, L., Spreafico, A., Chiabrando, F., Giulio Tonolo, F., 2022. Apple LiDAR Sensor for 3D Surveying: Tests and Results in the Cultural Heritage Domain. *Remote Sensing*, 14.

Trimble, 2022. https://geospatial.trimble.com/en/products/software/trimble-catalyst.

vigram, 2024. https://vigram.com/en/vidoc/.